Eur. Phys. J. A **1**, 365–378 (1998)

THE EUROPEAN PHYSICAL JOURNAL A

Study of the ^{90}Zr$(\vec{p},\alpha)^{87}$Y reaction at 22 MeV

P. Guazzoni[1], M. Jaskola[1,†], L. Zetta[1], J.N. Gu[2,‡], A. Vitturi[2], G. Graw[3], R. Hertenberger[3], P. Schiemenz[3], B. Valnion[3], U. Atzrott[4], G. Staudt[4]

[1] Dipartimento di Fisica dell'Università and Istituto Nazionale di Fisica Nucleare, via Celoria 16, I-20133 Milano, Italy
[2] Dipartimento di Fisica dell'Università and Istituto Nazionale di Fisica Nucleare, via Marzolo 8, I-35100 Padova, Italy
[3] Sektion Physik der Universität München, D-85748 Garching, Germany
[4] Physikalisches Institut der Universität, Auf der Morgenstelle 14, D-72076 Tübingen, Germany

Received: 17 November 1997
Communicated by D. Schwalm

Abstract. The $(\vec{p},\alpha)$ reaction on ^{90}Zr has been studied in a high resolution experiment at an incident proton energy of 22 MeV. The cross section and asymmetry angular distributions for transitions to 36 levels of ^{87}Y with an excitation energy up to 3 MeV have been measured. DWBA analyses of experimental angular distributions, using either Woods-Saxon or Double Folded potentials for the exit channel, have been done, allowing either the confirmation of previous spin and parity values or the assignment of new spin and parity to a large number of states. The structure of low lying states of ^{87}Y has been studied in the framework of the shell model, using the OXBASH code. With the interaction PMM90 reasonable agreement is obtained for part of the negative parity spectrum.

PACS. 21.60.Fw Models based on group theory – 21.60.Ev Collective models – 27.60.+j $90 \leq A \leq 149$ – 25.40.Hs Transfer reactions – 21.60.Cs Shell model

1 Introduction

The $(\vec{p},\alpha)$ reaction has often been used as a spectroscopic tool to investigate nuclear structure properties. For the theoretical description of the three-nucleon transfer processes the cluster model and different microscopic models have been applied. A review of the theory and references to relevant experimental and theoretical papers may be found in [1].

The ^{90}Zr(p,α)^{87}Y reaction has already been studied in experiments with low energy resolution and unpolarized protons [2], thus losing the possibility of unequivocally identifying the spin and parity of most of the excited levels. In fact the strong dependence of the asymmetry angular distributions of the emitted α-particles on the transferred total angular momentum J is of greatest importance to identify spin and parity of the levels excited in a $(\vec{p},\alpha)$ reaction, as shown in our previous studies on ^{208}Pb$(\vec{p},\alpha)^{205}$Tl and ^{209}Bi$(\vec{p},\alpha)^{206}$Pb [3–5].

Our aim in studying the ^{90}Zr$(\vec{p},\alpha)^{87}$Y reaction was not only to improve the experimental information available on the ^{87}Y levels but also to obtain accurate values of differential cross section ($\sigma(\theta)$) and asymmetry ($A_y(\theta)$) angular distributions for comparison with those measured at the same energy for ^{91}Zr$(\vec{p},\alpha)^{88}$Y [6]. For this reaction we have shown that the unpaired 51^{st} $d_{5/2}$ neutron in the target nucleus acts as a spectator. Therefore some of the higher excitation energy states of ^{88}Y, homologous to ^{87}Y states [6,7], result from the coupling of the 51^{st} neutron with the configurations excited in the ^{87}Y core. Moreover, in a recent analysis [8] of the ^{90,91}Zr(p,α)^{87,88}Y reaction continuous spectra, measured at low resolution, the extent to which the unpaired neutron in ^{91}Zr acts as spectator is assessed.

The level structure of ^{87}Y has been evidenced by different kinds of experimental results. In-beam γ-ray spectroscopy has been applied using the reactions ^{86}Sr(p,γ)^{87}Y [9], ^{88}Sr(p,2nγ)^{87}Y, ^{85}Rb(α,2nγ)^{87}Y [10] and ^{74,76}Ge(^{18}O,xn,yp,z$\alpha\gamma$) [11,12]. ^{87}Y isobaric analog resonances have been studied in polarized and unpolarized proton scattering from the target nucleus ^{86}Sr [13,14]. One- and multi-nucleon transfer reactions ^{86}Sr(^{3}He,d)^{87}Y [15], ^{89}Y(p,t)^{87}Y [16–18], ^{84}Sr(α,p)^{87}Y [19] and the previously referred ^{90}Zr(p,α)^{87}Y reaction [2] have also been used. The experimental results achieved are summarized in ref. [20].

In the present paper states in ^{87}Y have been populated via the ^{90}Zr$(\vec{p},\alpha)^{87}$Y reaction at 22 MeV bombarding energy. Accurate measurement of the differential cross sections and analyzing powers for transitions to 36 excited states of the ^{87}Y nucleus, in a high energy resolution ex-

† *guest researcher, permanent address:* Soltan Institute for Nuclear Studies, Swierk, Poland.
‡ *guest researcher, permanent address:* Institute of Modern Physics, Academia Sinica, Lanzhou, P.R.China.

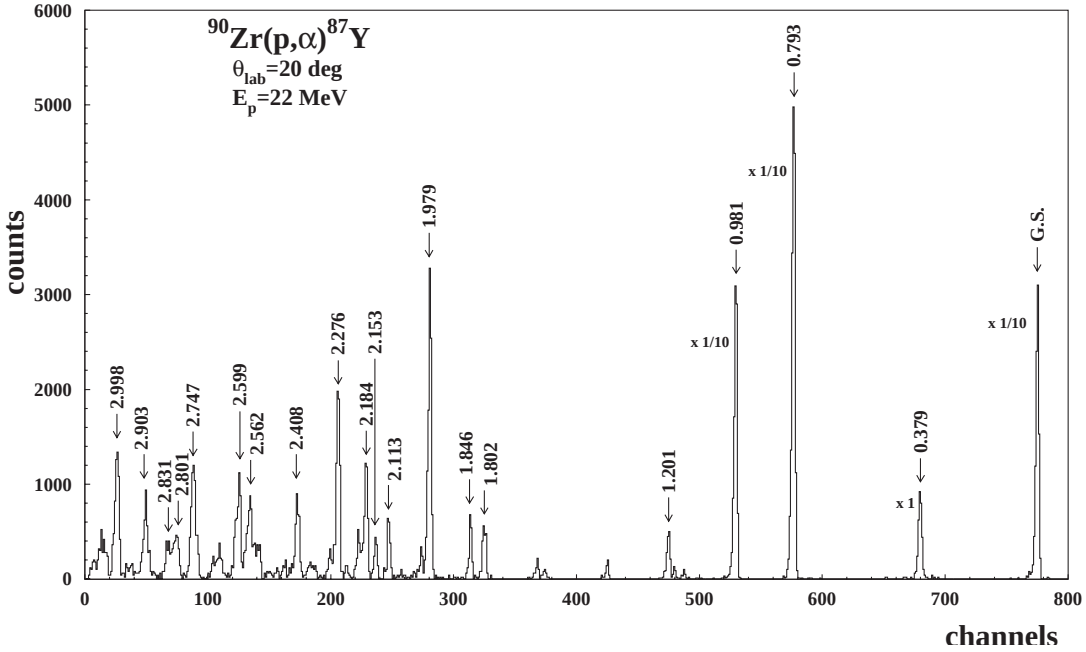

Fig. 1. Position spectrum of α particles measured at 20^o. For some levels the excitation energy is indicated

periment, allowed us to identify spin and parity for many levels.

In connection with the experimental work presented here, theoretical predictions of the energy spectrum, in the framework of the shell model, are presented for the ^{87}Y nucleus.

In Sect. 2 the experimental apparatus is described; Sect. 3 compares the experimental results and DWBA calculations, using both Woods-Saxon and Double-Folded potentials for the exit channel. In Sect. 4 spin and parity attributions are discussed, while Sect. 5 is devoted to shell model calculations. Section 6 presents the conclusions.

Preliminary reports of the present work are given elsewhere [7].

2 Experimental procedure and results

A beam of polarized protons, with an energy of 22 MeV, was produced by the Lamb shift ion source of the Munich HVEC MP Tandem accelerator. The ^{90}Zr target used was 50 μg/cm^2 thick, with an enrichment $\sim$ 97%, evaporated on a 6 μg/cm^2 Carbon backing. Outgoing α-particles have been detected in the focal plane of the Q3D magnetic spectrograph by the position and angle resolving light ion detector, with single wire proportional detectors and cathode periodic readout [21].

Angular distributions of cross section and asymmetry were measured from 5^o to 65^o, in steps of 5^o, with either spin-up or spin-down polarization, in two different magnetic field settings, to cover an excitation energy of the residual nucleus of $\sim$ 3.2 MeV. A Q3D solid angle of 11.04 msr was used for all the angles, except for θ=5^o,(2.98msr). The beam current was $\sim$140 nA; using the spin filter mode, the sign of the polarization (73$\pm$5)% was changed without any steering of the beam. Absolute cross sections were determined taking into account effective target thickness, solid angle and collected charge and are estimated with a systematic uncertainty of $\pm$15%. Areas and centroids of α-particle peaks were determined by using the code Autofit [22]. The shape of the α-peak at E$_x$=1.979 MeV was used as reference for both spin-up and spin-down spectra.

In order to calibrate the energy scale of the α-spectra, polynomials of rank 3 were used. The parameters corresponding to the two magnetic field settings were fixed in the energy range 0 to $\sim$3200 keV, imposing the reproduction of the following adopted levels [20]: 380.79, 793.60, 981, 1202.51, 2111.1, 2278, 2409 and 2995.2 keV. Our quoted energies are estimated to have an uncertainty of $\pm$3 keV. The good energy resolution obtained of $\sim$12 keV FWHM, essentially due to the target thickness, and the lack of any background allowed the identification of all observed peaks, even those with low cross section.

In Fig. 1 the α particle position spectrum measured at $\theta = 20^o$ is shown. This spectrum combines the measurements of the two magnetic settings used. The excitation energies of the most prominent peaks are indicated.

Differential cross sections $\sigma(\theta)$ and analyzing powers A$_y(\theta)$ for transitions to 36 levels of ^{87}Y have been obtained.

The excitation energies, spins and parities of the ^{87}Y levels of the present work are shown in Table 1, together with those from previous (p,α) experiments [2] and with the corresponding adopted values [20]. In the last column of the table the experimental cross sections, integrated from 5^o to 65^o, are shown.

Table 1. Energies of ^{87}Y levels, with attributed spins and parities, compared with those observed in previous (p,α) reaction [2] and with the corresponding adopted values [20]. In the last column the integrated cross sections from 5^o to 65^o are listed. The superscripts (A,B,C) of the J^π values of the present work indicate unambiguous and tentative assignments, and doublets, respectively

Present work		*(p, α) reactions* [2,20]		*Adopted levels* [20]		σ_{int}
$E_x(MeV)$	J^π	$E_x(MeV)$	J^π	$E_x(MeV)$	J^π	(μb)
0	$\frac{1}{2}^-$ A	0	$(\frac{1}{2}^-)$	0	$\frac{1}{2}^-$	56.0
0.379	$\frac{9}{2}^+$ A	0.377	$(\frac{9}{2}^+)$	0.381	$\frac{9}{2}^+$	13.3
0.793	$\frac{5}{2}^-$ A	0.790	$(\frac{5}{2}^-)$	0.794	$\frac{5}{2}^-$	119.0
0.981	$\frac{3}{2}^-$ A	0.976	$(\frac{3}{2}^-)$	0.981	$\frac{3}{2}^-$	143.8
1.151	$\frac{5}{2}^+$ A			1.153	$(\frac{5}{2})^+$	2.3
1.182	$\frac{3}{2}^-$ A	1.184	$(\frac{3}{2}^-)$	1.178	$(\frac{3}{2})^-$	2.9
1.201	$\frac{5}{2}^-$ A	1.200	$(\frac{5}{2}^-)$	1.202	$(\frac{5}{2})^-$	15.0
1.401	$\frac{13}{2}^+$ A	1.401		1.404	$(\frac{13}{2}^+)$	6.6
1.607	$(\frac{5}{2}^+, \frac{3}{2}^-)$ B	1.611		1.609	$\frac{3}{2}^-, \frac{5}{2}^-$	1.8
1.629	$\frac{5}{2}^+$ A			1.623	$(\frac{5}{2}, \frac{7}{2})$	4.9
1.704	$\frac{3}{2}^-$ A			1.704	$(\frac{5}{2}^-)$	1.1
1.757	$\frac{5}{2}^+$ A	1.763	$(\frac{5}{2}^-)$	1.757	$(\frac{5}{2}^+, \frac{7}{2}^-)$	1.7
1.802	$\frac{5}{2}^-$ A			1.801	$(\frac{1}{2}^-, \frac{3}{2}, \frac{5}{2}^-)$	8.8
1.846	$\frac{1}{2}^-$ A	1.850	$(\frac{3}{2}^-)$	1.851	$\frac{1}{2}^-$	4.0
1.979	$\frac{7}{2}^-$ A	1.990	$(\frac{9}{2}^-)$	1.988	$(\frac{7}{2}, \frac{9}{2})^-$	63.8
2.006	$\frac{11}{2}^+$ A			2.008	$(\frac{7}{2})$	20.6
2.113	$\frac{5}{2}^+$ A			2.111		14.4
2.153	$(\frac{9}{2}^-, \frac{11}{2}^+)$ B			2.159		15.5
				2.166	$(\frac{7}{2})^-$	
		2.170	$(\frac{7}{2}^-)$			
2.184	$\frac{7}{2}^-$ A			2.185		25.3
2.209	$\frac{3}{2}^-$ A			2.207	$(\frac{15}{2}^+, \frac{17}{2}^+)$	12.5
				2.210	$(\frac{1}{2})$	
				2.242	$(\frac{7}{2}, \frac{9}{2}^-)$	
2.249	$\frac{9}{2}^-$ A			2.244		2.9
				2.274	$(\frac{9}{2}^+)$	
2.276	$(\frac{7}{2}^+ + \frac{9}{2}^-)$ C	2.270	$(\frac{9}{2}^+)$	2.278	$(\frac{7}{2})^-$	52.2
2.302	$\frac{13}{2}^+$ A					14.6
				2.354		
2.365	$(\frac{15}{2}^- + \frac{7}{2}^+)$ C			2.367	$(\frac{15}{2})^-$	7.5
2.408	$\frac{3}{2}^-$ A	2.406	$(\frac{15}{2}^-)$	2.409	$(\frac{3}{2})^+$	18.4
2.449	$\frac{9}{2}^-$ A			2.446	$(\frac{5}{2})^+$	10.7
2.531	$\frac{11}{2}^-$ A			2.532		19.0
2.562	$\frac{11}{2}^+$ A			2.564	$(\frac{9}{2})^+$	56.0
				2.572	$(\frac{3}{2}^-)$	
2.599	$\frac{9}{2}^-$ A			2.595		37.4
				2.600	$(\frac{15}{2}^-)$	
				2.602	$(\frac{7}{2})^+$	
		2.630	$(\frac{13}{2}^-)$			
2.661	$\frac{7}{2}^+$ A					8.9
				2.668	$(\frac{5}{2})$	
2.682	$\frac{11}{2}^+$ A			2.676	$(\frac{17}{2})^-$	7.7
2.747	$\frac{3}{2}^+$ A					31.1
2.801	$(\frac{11}{2}^+ + \frac{3}{2}^+)$ C					12.7
				2.812	$\frac{9}{2}^+, \frac{11}{2}^+$	
				2.827	$(\frac{21}{2}^+)$	
				2.828	$(\frac{3}{2}^-, \frac{5}{2}^-)$	
2.831	$\frac{9}{2}^-$ A					10.9
2.903	$(\frac{3}{2}^-, \frac{5}{2}^+)$ B			2.901	$\frac{3}{2}^-, \frac{5}{2}^-$	25.5
		2.960	$(\frac{13}{2}^-)$			
2.998	$\frac{5}{2}^+$ A	2.999	$(\frac{5}{2}^+)$	2.995	$(\frac{5}{2})^+$	39.1

Table 2. Woods-Saxon optical model parameters for the incident proton and emitted α particle and geometrical parameters for the triton bound state used in DWBA calculations

	V_r (MeV)	r_r (fm)	a_r (fm)	W_v (MeV)	r_v (fm)	a_v (fm)	W_d (MeV)	r_d (fm)	a_d (fm)	V_{so} (MeV)	r_{so} (fm)	a_{so} (fm)	r_c (fm)
p	52.4	1.20	0.69	1.12	1.236	0.69	8.27	1.236	0.69	5.90	1.072	0.63	1.25
α	230.5	1.26	0.70	23.5	1.26	0.70							1.30
B.S.		1.4	0.4										

3 Distorted wave analysis

The angular distributions of cross section and asymmetry, obtained at 22 MeV incident energy exhibit features sufficiently prominent to make a distinction between different L-transfers. Furthermore, the dependence of $\sigma(\theta)$ and $A_y(\theta)$ on the transferred total angular momentum J allows the unique identification of most of the excited levels in ^{90}Zr$(\vec{p},\alpha)^{87}$Y reaction. Two different analyses of the experimental reaction data have been carried out. In the first analysis Woods-Saxon potentials have been used for the α channel whereas the second uses double-folded α-nucleus potentials.

The DWBA calculations with Woods-Saxon potentials in entrance and exit channels (see Table 2 for the set of parameters used) were carried out in the finite-range approximation with the code TWOFNR [23]. For the proton channel, the Varner et al. global nucleon-nucleus optical model potential is used [24]. The α-particle parameters, in Woods-Saxon parameterisation, are those suggested by Wit et al. [25], that correctly account for the overall structure and magnitude of the angular distributions of the α elastic-scattering from ^{89}Y. In addition to the potentials in the entrance and exit channel, the theoretical curves critically depend on the proper choice of the triton well radius and diffuseness parameters.

For the proton-triton interaction a potential of Gaussian form $V(r_{pt}) = V_0 \exp -(\frac{r_{pt}}{\xi})^2$ with $\xi = 1.42$ fm is used.

In the second analysis of the data, a double-folding procedure was used to derive the real part of the optical α-nucleus potential. The potential is described by [26]

$$U_F(\vec{r}) = \lambda \int d\vec{r}_1 \int d\vec{r}_2 \rho_T(\vec{r}_1)\rho_\alpha(\vec{r}_2)t(E,\rho_T,\rho_\alpha,\vec{s})$$

where $\vec{s} = \vec{r} + \vec{r}_2 - \vec{r}_1$, $\vec{r}$ is the separation of the centers of mass of the target nucleus and the α-particle, $\rho_T(\vec{r}_1)$ and $\rho_\alpha(\vec{r}_2)$ are the respective nucleon densities, and λ is an overall normalization factor. For the effective interaction t, the density-dependent form of the M3Y nucleon-nucleon interaction has been chosen. The target nucleus density distribution ρ_T was the experimental one [27] obtained from electron scattering and unfolded from the finite-charge distribution of the proton. For the density distribution of the α-particle, a Gaussian form was used [28]. Details of the numerical computation of the potential $U_F(\vec{r})$ are described in [29]. As imaginary part, a volume Woods-Saxon potential was chosen. The DWBA calculations were made again in the finite-range approximation, however in this case with the computer code DWUCK5 [30]. First, the angular distribution of the ground-state transition has been fitted with the code TROMF [31], which allows a simultaneous fit to both the elastic-scattering data in the entrance and exit channels and to the reaction data [32]. For the proton channel the experimental data from Ball et al. [33] at $E_p = 22.5$ MeV were used. The Woods-Saxon potential parameters for the proton channel resulting from the simultaneous fit are nearly identical with those deduced by Varner et al. [24] listed in Table 2. The scattering data in the exit channel proved to be more difficult. The nucleus ^{87}Y is unstable, therefore elastic scattering data from neighbouring isotopes had to be used. Since the α-^{89}Y elastic scattering data measured by Wit et al. [25] do not cover scattering angles smaller than $\theta_{CM} < 40^o$, the potentials resulting from the simultaneous fit were not in concordance with the global α-nucleus potential deduced recently [34]. Therefore α-^{89}Y data measured by England et al. [35] at E_α= 25 MeV were used. Since only weak energy dependence of the α-nucleus potential has been found for α energies near 25 MeV [34], the use of these data in the simultaneous fits is justified. The form factors for the heavy and light particles (HPFF and LPFF, respectively) are calculated using Woods-Saxon potentials. The numbers of nodes in the radial bound-state wave function (HPFF) is given by the conservation rule for the harmonic oscillator quanta

$$Q = (2n_p + l_p) + 2(2n_n + l_n) = 2N_t + L_t$$

where n_i and l_i are the quantum numbers of the individual nucleons which form the triton cluster. The three transferred nucleons are supposed to be in a relative l=0 state. Assuming a ground state configuration $\pi(p_{1/2})^{-1}$ $\nu(g_{9/2})^{-2}$ for ^{87}Y, one obtains Q=11 and N=5 as number of nodes. The parameters found in the simultaneous fit are listed in Table 3 together with the resulting values for the volume integrals and the rms radii.

The results of the fitting procedure with respect to the elastic scattering data are shown in Fig. 2, the simultaneously fitted g.s. reaction cross section is shown in Fig. 3. With the potentials and the form factor parameters reported in Table 3, calculations of cross sections and analysing powers for all measured transitions were carried out using the code DWUCK5 [30]. The experimental data and the results of the calculations using both conventional Woods-Saxon and double-folded α-particle potentials are compared in Figs. 3–9.

The shapes of the experimental $\sigma(\theta)$ and $A_y(\theta)$ angular distributions are reproduced in the two different analyses

Table 3. Values of the normalization factor λ, the parameters of the imaginary Woods-Saxon α-nucleus potential used with the double-folded real potential, the geometrical parameters of the form factor and the resulting values of the volume integrals and rms radii

	λ	r_r (fm)	a_r (fm)	W_v (MeV)	r_v (fm)	a_v (fm)	J_R $(MeVfm^3)$	$< r_R^2 >^{1/2}$ (fm)	J_I $(MeVfm^3)$	$< r_I^2 >^{1/2}$ (fm)
α	1.204			8.326	1.83	0.576	362.7	5.051	54.5	6.537
t		1.23	1.19							

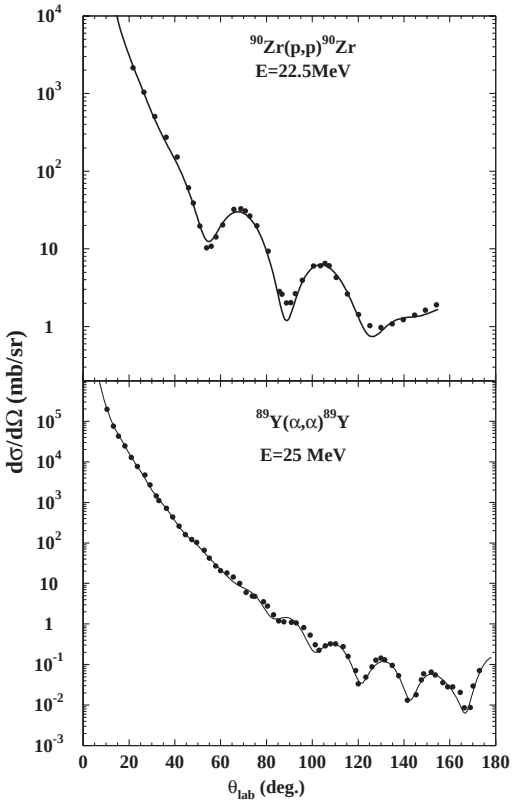

Fig. 2. Differential cross sections in the entrance and exit channels. The experimental data, taken from [33] and [35] respectively, are given by *circles*. The *solid lines* are optical model theoretical estimations obtained using, for protons elastic scattering on ^{90}Zr, Woods-Saxon potential parameters listed in Table 2 and for α elastic scattering on ^{89}Y, double-folded potential parameters listed in Table 3

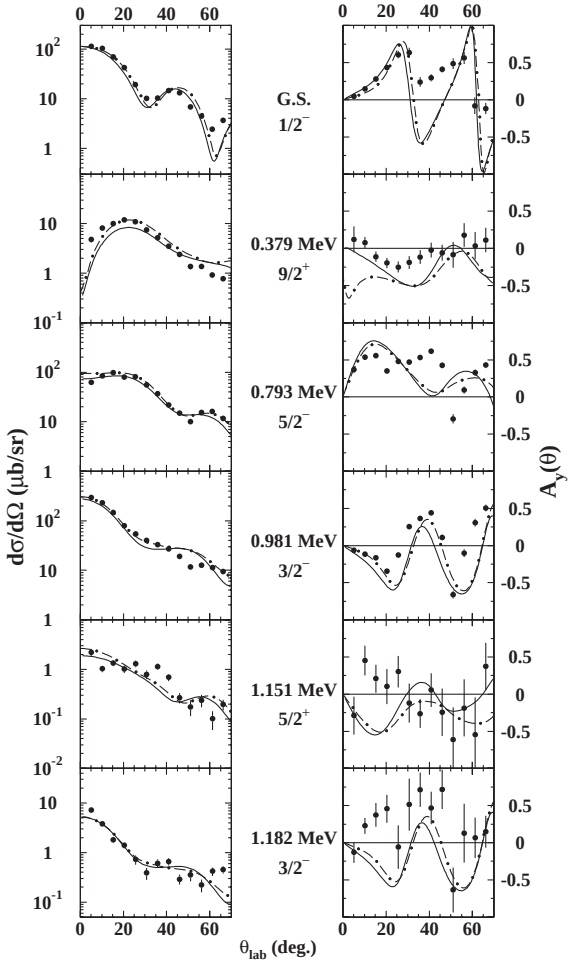

Fig. 3. Angular distributions and analyzing powers for the transitions to the levels whose excitation energy, spin and parity are indicated. The *dots* represent the experimental data, the *dot-dashed lines* the theoretical estimates obtained with the double-folded α particle potential, and the *solid lines* the theoretical estimates obtained with the conventional Woods-Saxon potential. The energies attributed to the observed levels are those given in the present work

with comparable accuracy. They are almost indistinguishable, also in the case of transitions to high-spin levels at higher excitation energies.

4 Spin and parity attributions

For identifying the spin and parity of the levels populated in a $(\vec{p},\alpha)$ reaction, the noticeable dependence on the transferred total angular momentum J, displayed by the angular distributions of cross sections $\sigma(\theta)$ and, in a larger degree, of analyzing powers $A_y(\theta)$ [3–7,36,37], appears to be of the greatest importance.

Moreover, the following distinctive feature of the analyzing power is a useful tool for the spin and parity attribution: for negative parity states, at forward angles $A_y(\theta)$ jumps from mainly positive to mainly negative values with J increasing, and for the same J the sign of $A_y(\theta)$ changes as well, if the parity is inverted.

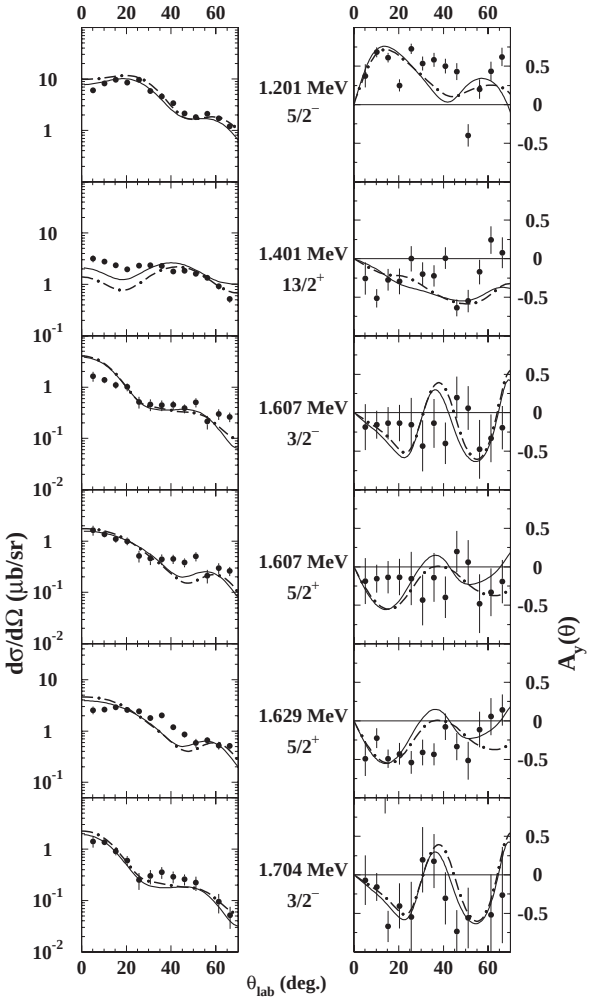

Fig. 4. Same as Fig. 3

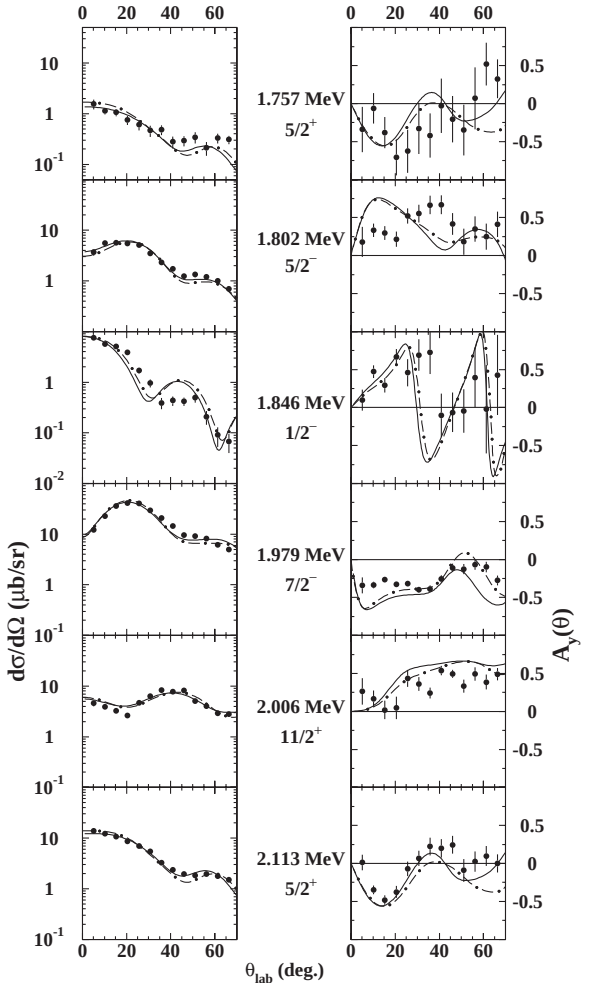

Fig. 5. Same as Fig. 3

In the present case of ^{90}Zr($\vec{p},\alpha$)^{87}Y, at the incident proton energy of 22 MeV, the J transfer dependence is particularly prominent and, in addition, the high absolute values of the analyzing power allow its measurement, in a high resolution experiment using a thin target, though the corresponding $\sigma(\theta)$ are small.

In order to assign proper spin and parity values to each level, DWBA calculations were carried out both for the adopted J^π values (where present) and for several other possible values of J^π. The assumed values derive from a best fit to the experimental angular distributions. For the unambiguous assignments given in the present work, the shape difference among the DWBA curves corresponding to the chosen values of J^π and the other tested values is in any case large enough to allow an unambiguous assignment.

Up to the 0.981 MeV $3/2^-$ level, the spins and parities attributed on the basis of the comparison between the measured angular distributions and the theoretical predictions agree with the values reported on the adopted level scheme [20] and up to 1.401 MeV we confirm, without uncertainty, the tentative attributions of the adopted level scheme [20].

1.607 MeV level. On the adopted level scheme [20], a level is reported at an energy of 1.609 MeV, on the basis of the study of the ^{89}Y(p,t)^{87}Y [17] (L=2 transfer from $J^\pi=1/2^-$ target) and a value of $3/2^-$, or $5/2^-$, is given. From a study of $\sigma(\theta)$ in the ^{86}Sr(^{3}He,d)^{87}Y [15], a level with an energy of 1.605±0.025 MeV was found to which a spin and parity of $9/2^+$ was attributed. The 1.607 MeV level in the present ($\vec{p},\alpha$) reaction is quite weakly populated and the measured values of $A_y(\theta)$ are characterized by large errors. The experimental angular distributions of $\sigma(\theta)$ and $A_y(\theta)$ are reproduced by $J^\pi=5/2^+$, or with almost the same accuracy by $J^\pi=3/2^-$.

1.629 MeV level. On the adopted level scheme [20], a level is reported at an energy of 1.623 MeV, on the basis of ^{85}Rb(α,2nγ)^{87}Y [10] reaction studies with tentative spin (5/2, 7/2). Medsker et al., from a study of $\sigma(\theta)$ in the ^{84}Sr(α,p)^{87}Y [19], report a level with energy of 1618±8 keV, to which they attribute a spin and parity ($9/2^+$). A satisfactory fit to both $\sigma(\theta)$ and $A_y(\theta)$ is obtained in the present experiment by assuming $5/2^+$ for the spin and parity.

1.704 MeV level. The adopted spin and parity for this level are ($5/2^-$), obtained from a γ-ray study. The $\sigma(\theta)$

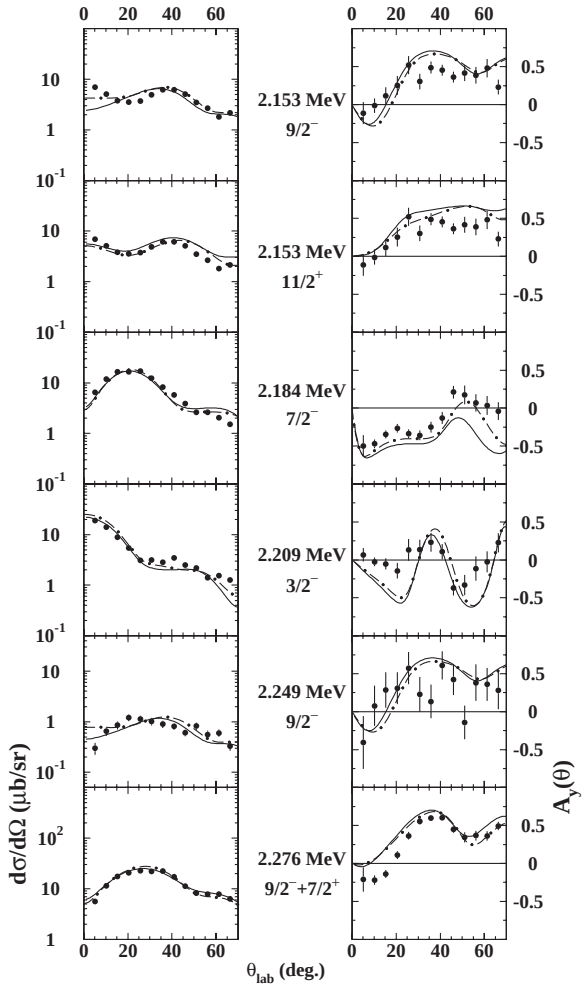

Fig. 6. Same as Fig. 3

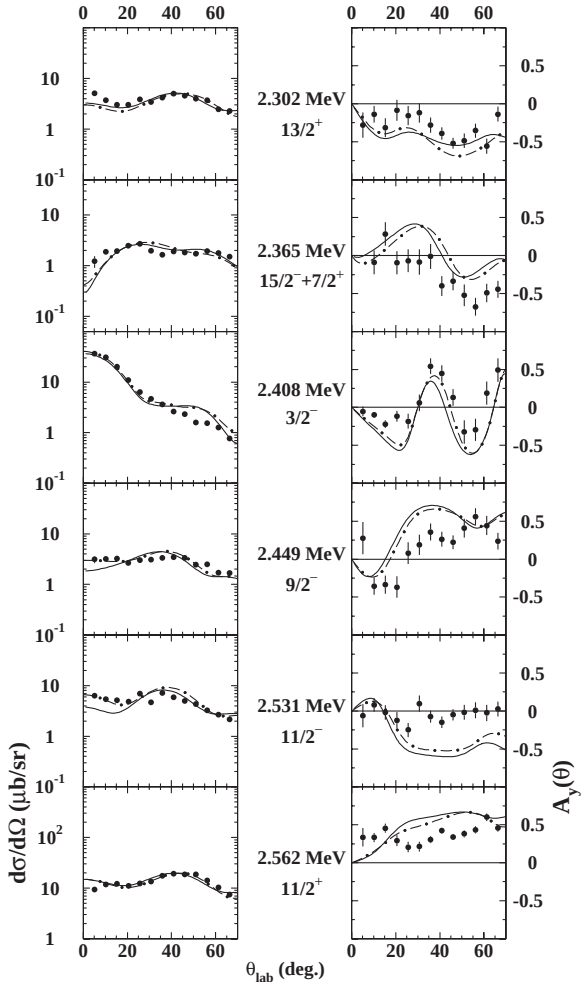

Fig. 7. Same as Fig. 3

and $A_y(\theta)$ measured by us are quite satisfactorily reproduced by assuming a value of $3/2^-$ for the spin and parity. This level is quite weakly populated and the measured values of $\sigma(\theta)$ and $A_y(\theta)$ are characterised by large errors.

1.757 MeV level. The adopted spin and parity for this level are ($5/2^+$, $7/2^-$) on the basis of γ-ray studies. A satisfactory reproduction of both $\sigma(\theta)$ and $A_y(\theta)$ is obtained by assuming a value of $5/2^+$. Also this level is quite weakly populated and the measured values of $\sigma(\theta)$ and $A_y(\theta)$ are characterised by large errors.

1.802 MeV level. On the adopted level scheme [20], a level with energy 1801 keV is listed with spin and parity ($1/2^-$, $3/2$, $5/2^-$) on the basis of γ-ray studies. In the present experiment the assumption $5/2^-$ provides a reproduction of angular distributions that is accurate for cross-section and reasonable for asymmetry.

1.846 MeV level. On the adopted level scheme [20], a level with energy 1851±3 keV is listed as the weighted average value from (^{3}He,d) [15], (p,t) [17], (α,p) [19] reaction studies. The spin and parity reported are $1/2^-$ on the basis of the $\sigma(\theta)$ measured in (p,t) reaction [18]. The $1/2^-$ attribution is confirmed by our analysis since it provides a good reproduction of $A_y(\theta)$ and a reasonably good reproduction of $\sigma(\theta)$.

1.979 MeV level. On the adopted level scheme [20], a level at 1988±5 keV is reported with spin and parity $(7/2, 9/2)^-$, as suggested by the analysis of the (p,t) [18] and (p,α) [2] reactions and by γ-ray studies. The $7/2^-$ attribution is confirmed by our analysis, since it provides an accurate reproduction of both $\sigma(\theta)$ and $A_y(\theta)$.

2.006 MeV level. A level at 2007.91 keV is cited on the adopted level scheme with spin (7/2) from the (p,2nγ) study [10]. A perfect reproduction of $\sigma(\theta)$ and a satisfactory one for $A_y(\theta)$ is obtained by assuming a value of $11/2^+$ for spin and parity.

2.113 MeV level. On the adopted level scheme, a level at 2111.1±0.8 keV is listed without spin and parity assignment, from (p,γ) studies. However, from ^{89}Y(p,t)^{87} [18] a level at 2122±5 keV, with L=3 transfer and possible spin and parity $5/2^+$ or $7/2^+$, is found. We find a perfect reproduction of both $\sigma(\theta)$ and $A_y(\theta)$ for a $5/2^+$ assignment.

2.153 MeV level. On the adopted level scheme [20] a level at 2158.9 keV is reported without spin and parity assignment, from γ-ray studies. In our analysis, $9/2^-$ or

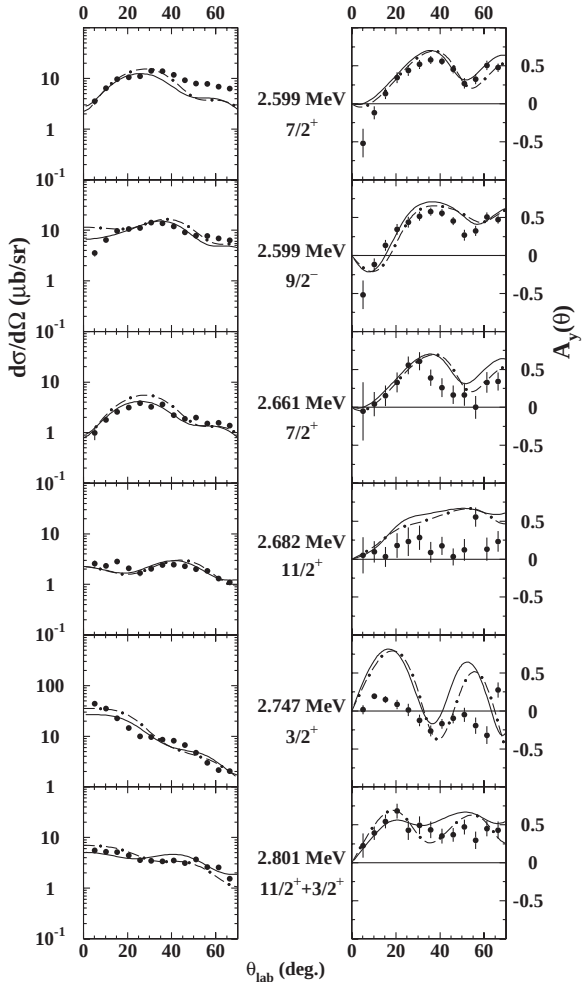

Fig. 8. Same as Fig. 3

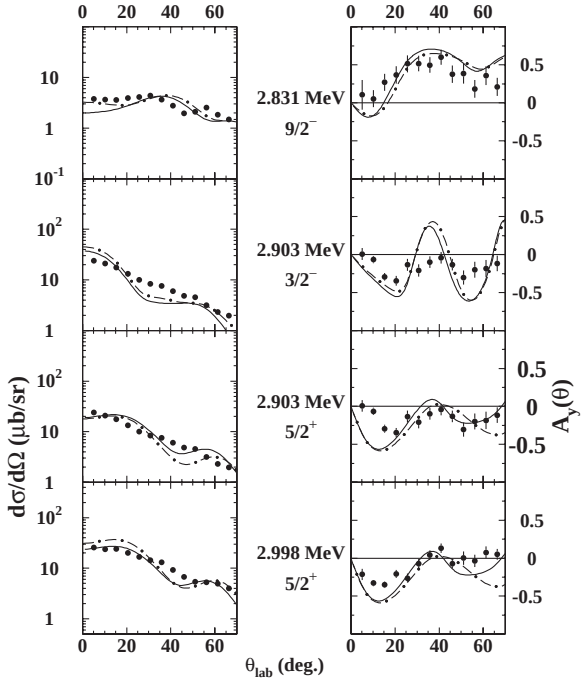

Fig. 9. Same as Fig. 3

$11/2^+$ attributions give accurate reproduction of $\sigma(\theta)$ and $A_y(\theta)$.

2.184 MeV level. A level with an energy 2166±5 keV is reported as the weighted average value of 2165±5 keV from (p,t) [18] and 2170±10 keV from (p,α) [2] with possible spin and parity of $(7/2)^-$, while a level at 2185.0 keV is given without spin and parity assignment on the basis of γ-ray studies [20]. We reproduce perfectly both angular distributions by attributing spin and parity $7/2^-$.

2.209 MeV level. On the adopted level scheme [20], there is a group of levels with energies from 2201.7 to 2216 keV, with different spin and parity assignments. The attribution $3/2^-$ for this level leads to an accurate reproduction of $\sigma(\theta)$ and $A_y(\theta)$.

2.249 MeV level. On the adopted level scheme, there are three levels nearby, the first at 2241.7 keV with (7/2, $9/2^-$) assignment, the second at 2244.2 keV, without spin and parity assignment, both from β- and γ-ray studies [20], and a third level at 2256 keV from the (p,t) reaction [18] with a possible attribution of $3/2^-$ or $5/2^-$. An assignment of $9/2^-$ provides a reasonable reproduction for $\sigma(\theta)$ and for $A_y(\theta)$. This level is quite weakly populated and the measured angular distributions are characterized by large errors.

2.276 MeV level. A level at 2.274 MeV with $(9/2^+)$ attribution and a level at 2.278 MeV with spin and parity $(7/2)^-$, from (^{3}He,α) [15] and (α,p) [19] reaction studies are reported in the adopted level scheme [20]. In our case a $9/2^-$ value provides a poor reproduction for $\sigma(\theta)$ and a good one for $A_y(\theta)$, while the $7/2^+$ value provides a good reproduction of $\sigma(\theta)$ and satisfactory one for $A_y(\theta)$. A better reproduction of both cross section and asymmetry angular distributions can be obtained by considering an unresolved doublet of one level of spin and parity $9/2^-$ (30%) and another one of spin and parity $7/2^+$ (70%).

2.302 MeV level. No level is given at this energy by the adopted level scheme [20]. In our case $\sigma(\theta)$ and $A_y(\theta)$ are reasonably reproduced by attributing $13/2^+$ to this level.

2.365 MeV level. A level at 2354.5 keV, without spin and parity and a level at 2366.8±0.14 keV with attributed spin and parity $(15/2)^-$ on the basis of γ-rays studies [10, 12] are given by the adopted level scheme [20]. Oelrich et al. [18] find, from a (p,t) study of $\sigma(\theta)$ a level at 2374±5 keV with L=8 transfer from a $J^\pi=1/2^-$ target nucleus. We obtain a good reproduction of cross section and asymmetry angular distributions by considering an unresolved doublet of one level of spin and parity $15/2^-$ (90%) and another one of spin and parity $7/2^+$ (10%).

2.408 MeV level. On the adopted level scheme [20] a level with an energy of 2.409 MeV is reported with spin and parity $(3/2)^+$, on the basis of (p,t) [18], (^{3}He,d) [15] and γ-ray studies. We reproduce accurately both angular distributions by assuming a value of $3/2^-$ for spin and parity.

2.449 MeV level. On the adopted level scheme a level is given with an energy of 2.446 MeV on the basis of (p,t) [18] and γ- ray studies [20] and with spin and parity $(5/2)^+$. This attribution leads to a very poor reproduction of the measured angular distributions. The $\sigma(\theta)$ and $A_y(\theta)$ are compatible with the attribution of $J^\pi=9/2^-$.

2.531 MeV level. On the adopted level scheme [20] a level at an energy of 2.532 MeV is reported without spin and parity attribution. The cross section angular distribution is quite accurately reproduced by attributing $J^\pi=11/2^-$ to this level. The measured $A_y(\theta)$ is less accurately reproduced, being very small (about zero starting from 30^o).

2.562 MeV level. A level at 2563.9±0.8 keV with attributed spin and parity $(9/2)^+$ on the basis of γ-ray and of (p,t) [18] studies is listed on the adopted level scheme [20]. This attribution leads to a very poor reproduction for the measured $\sigma(\theta)$ and a completely wrong prediction for $A_y(\theta)$. We obtain a very good reproduction of $\sigma(\theta)$ by assuming a value of $11/2^+$. The positive measured asymmetry is consistent with this attribution.

2.599 MeV level. On the adopted level scheme [20] there is a group of levels with energies: 2595 keV, without spin and parity attribution, 2600 keV, with attribution $(15/2^-)$ from (p,α) studies [2] and at 2.602 MeV with $(7/2)^+$attribution. A quite accurate reproduction of the angular distribution and asymmetry is obtained by assuming for this level a spin and parity value of $9/2^-$.

2.661 MeV level. The adopted level scheme [20] reports a level at 2.668 MeV (5/2), from comparison of primary γ strength with the γ strength to the 0.381 MeV level in (p,γ) reaction. We reproduce quite accurately the measured angular distribution and asymmetry by assuming a value of $7/2^+$ for this level.

2.682 MeV level. A level at 2675.90±0.16 keV with attributed spin and parity $(17/2)^-$ on the basis of γ-ray studies from the (α,2nγ) reaction [10] is listed on the adopted level scheme [20]. This attribution is incompatible with our findings, since it would give rise to a $\sigma(\theta)$ peaked at about 60 ^{o}. The cross section and asymmetry are compatible with the attribution of $11/2^+$, also taking into account that most of the measured values of the asymmetry are near zero.

2.747 MeV level. No level is given at this energy on the adopted level scheme. This level is populated quite strongly and the measured values of $\sigma(\theta)$ and $A_y(\theta)$ are characterized by small errors. We reproduce quite accurately the cross section and reasonably we reproduce the asymmetry, by assuming a value of $3/2^+$ for spin and parity.

2.801 MeV level. The observed level (or levels) is populated quite strongly, but at this energy the adopted level scheme [20] does not report any level, while it reports a level at 2812.2±1 keV from β-decays and from (p,t). Oelrich et al. [18] from (p,t) reaction studies observe a level at 2808±5 keV with L=5 transfer from a $J^\pi=1/2^-$ target. We can not obtain a satisfactory agreement between observed and computed angular distributions by considering only one contributing level. We obtain a good reproduction for $\sigma(\theta)$ and $A_y(\theta)$ by considering an unresolved doublet, i.e. one level with $J^\pi=11/2^+$ (80%) and another one with $J^\pi=3/2^+$ (20%).

2.831 MeV level. Near to this energy in the adopted level scheme [20] there are two levels with similar energies, one at 2.827 MeV with spin and parity $(21/2^+)$ assigned on the basis of the γ-ray studies [9,11] and the other at 2.828 MeV with possible spin and parity values ($3/2^-$, $5/2^-$) assigned from a (p,t) study [18] as L=2 transfer from $J^\pi=1/2^-$ target nucleus. Our observed level is populated relatively strongly with small errors and we reproduce accurately the cross section and asymmetry angular distributions, assuming that this transition corresponds to a level with spin and parity $J^\pi=9/2^-$.

2.903 MeV level. The adopted level scheme [20] gives a level at 2901±5 keV with possible spin $3/2^-$, $5/2^-$, (L=2 transfer from $J^\pi=1/2^-$ target in (p,t) reaction [18]). The observed level is strongly populated and the overall fit of $\sigma(\theta)$ and $A_y(\theta)$ indicates $J^\pi=3/2^-$ or $5/2^+$.

2.998 MeV level. On the adopted level scheme [20] there is a group of 4 levels with energies from 2995 to 2996.2 keV with different attributions of spins and parities, in parenthesis. To the level at 2995±2 keV, on the basis of (^{3}He,d) [15] and (p,α) [2] studies, is attributed spin and parity $(5/2^+)$. This level is populated very strongly in our measurement. We find a reasonably good reproduction of both asymmetry and cross section by taking $J^\pi=5/2^+$.

5 Shell model calculations and the structure of ^{87}Y

As is well known, the structure of nuclei around A ≈ 88–90 is particularly interesting from the point of view of the shell structure. The role of the intruder $g_{9/2}$ orbital, the possible proton closure at Z=38 or 40 and the subsequent effect of particle-hole excitations, as well as the onset of deformation, have been debated at length. Up till now a fully consistent treatment of these systems with regards to the different observables (energies, e.m. transitions, one- and many-particle spectroscopic factors, etc.) has not been obtained. Quite a number of shell model calculations have been performed in this region, within different model spaces and with different interactions. However, most interest has been often placed on systematic overall properties as a function of the mass, or on detailed calculations for specific key nuclei, as ^{90}Zr [38]. In our case, trying to contribute to a better understanding of this region, we have supplemented the present ($\vec{p}$, α) data with more specific shell model calculations for ^{87}Y nucleus, not restricted to the lower energies or spins, with alternative choices of the residual interaction.

The necessary inputs for the calculations are the single-particle energies and the two-body matrix elements in the shell-model Hamiltonian

$$H = \sum_i \epsilon_i a_i^\dagger a_i + \sum_{ijkl} V_{ijkl}\ a_i^\dagger a_j^\dagger a_k a_l \ ,$$

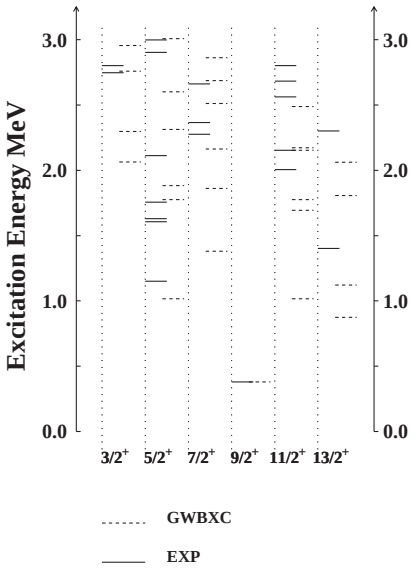

Fig. 10. The results for the positive parity states of ^{87}Y obtained with the GWBXC interaction are compared with the experimental energy levels identified in the present experiment

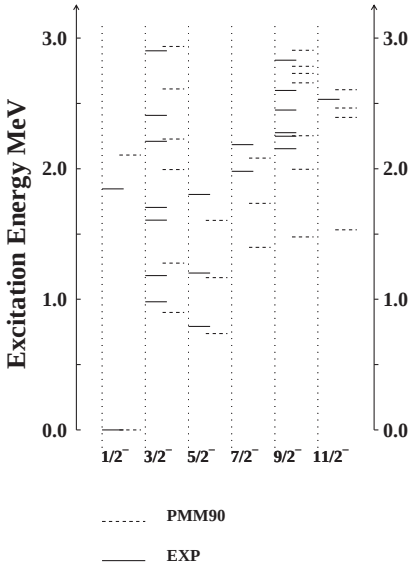

Fig. 11. The results for the negative parity states of ^{87}Y obtained with the PMM90 interaction are compared with the experimental energy levels identified in the present experiment

as well as the choice of the model space. We have performed two calculations, using the large-basis shell model code OXBASH [39].

The first is based on the GWBXC interaction [40], which is an effective G-matrix interaction derived from the Paris nucleon-nucleon interaction. In this case the model space has been chosen by correlating the protons in $1f_{5/2}[5-6]$, the $2p_{3/2}[3-4]$, $2p_{1/2}[0-2]$ and $1g_{9/2}[0-1]$ orbitals and the neutrons in the $1g_{9/2}[8]$ orbital. The numbers in the square brackets give the allowed occupation numbers for each orbital. For ^{87}Y this means that the considered configurations have a proton component of $1h$ character for the negative-parity states (with respect to the $Z = 40$ subshell) and of $1p-2h$ character for the positive-parity states.

The single particle energy values used in the calculations are: $1f_{5/2}$ -8.90 MeV, $2p_{3/2}$ -12.62 MeV, $2p_{1/2}$ -9.61 MeV, $1g_{9/2}$ -5.07 MeV for protons and for neutrons $1g_{9/2}$ 0.664 MeV. They have been taken to correspond to the experimental single particle values around ^{90}Zr.

In Fig. 10 the results for the positive parity states of ^{87}Y obtained with the GWBXC interaction are compared with the experimental energy levels identified in the present experiment.

The second calculation has been performed with the PMM90 interaction [39], which was introduced by B.A.Brown. In this latter case, both neutrons and protons have been assumed to move in the $1f_{5/2}[11-12], 2p_{3/2}[7-8], 2p_{1/2}[2-4]$ and $1g_{9/2}[8-10]$ orbitals. In this case the allowed occupation numbers refer to the total neutron plus proton occupancy. This latter choice of the model space for the negative-parity states allows the inclusion, not only of the $1h$ states, but also of the $2p-3h$ states which, if one considers as subshells Z, N=40, correspond to particle-hole excitations for both the proton and neutron components or for a proton (and/or neutron) double particle-hole excitation. For the positive-parity states, on the other hand, the configuration space is close to the case of the GWBXC interaction, with states of $1p-2h$ character.

The single particle energy values, in the case of PMM90 interaction, are $1f_{5/2}$ 2.30 MeV, $2p_{3/2}$ 3.40 MeV, $2p_{1/2}$ 5.13 MeV, $1g_{9/2}$ 2.75 MeV. They are different from the previous case and have been adjusted [39] to account for the radical changes in the residual two-body matrix elements.

In Fig. 11 the results for the negative parity states of ^{87}Y obtained with the PMM90 interaction are compared with the experimental energy levels identified in the present experiment.

All the calculated energy levels obtained with the GWBXC and PMM90 interactions are summarized in Fig. 12 together with the corresponding experimental energy levels seen in the present work.

Let us first comment on the results obtained with the GWBXC interaction for the low-lying states. The main components of the wave functions for a few selected states with negative and positive parity are given in Table 4 and 5 respectively. One can see that the ground-state $1/2^-$ corresponds to an essentially pure hole-state in the $2p_{1/2}$ orbital. Similarly, the $9/2^+$ state is a dominantly pure particle state in the $g_{9/2}$ orbital, with two holes in the $p_{1/2}$ orbital.

Conversely, the lowest $3/2^-$ and $5/2^-$ states do not correspond to dominant configurations associated with one hole in the $p_{3/2}$ or $f_{5/2}$ orbitals (this character being instead associated with the second $3/2^-$ and $5/2^-$ states). These yrast states correspond to the energetically favoured situation in which the proton hole is still in the $p_{1/2}$ orbital, but associated with a recoupling to J=2 of a

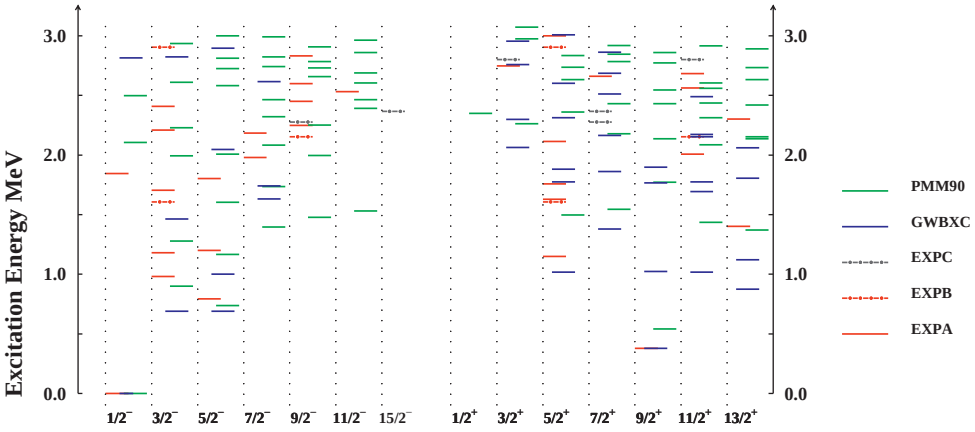

Fig. 12. Energy level scheme for ^{87}Y. The figure shows all the results obtained using the GWBXC (*blu lines*) and PMM90 interaction (*green lines*) compared with the levels observed in the present experiment: *red lines* (EXPA) indicate the levels with unambiguous assignment of J^{π}, *red solid dotted lines* (EXPB) the levels with tentative assignment and *grey solid dotted lines* (EXPC) the doublets

Table 4. Energy eigenvalues and percentage of different components (squared amplitudes) obtained within the Shell Model Hamiltonian with GWBXC interaction for low lying negative parity states of ^{87}Y. [NO] is the number of unpaired nucleons

E(th)	0.000	0.691	0.689	1.464	1.000	Orbit partition order				
[NO]	$1/2^-$	$5/2^-$	$3/2^-$	$3/2^-$	$5/2^-$	$\pi f_{5/2}$	$\pi p_{3/2}$	$\pi p_{1/2}$	$\pi g_{9/2}$	$\nu g_{9/2}$
[1]	7.81	39.59	4.62	10.92	69.74	5	4	2	0	8
[1]	5.14	3.01	17.70	78.21	3.61	6	3	2	0	8
[1]	87.05	57.39	77.68	10.87	26.65	6	4	1	0	8

Table 5. Energy eigenvalues and percentage of different components (squared amplitudes) obtained within the Shell Model Hamiltonian with GWBXC interaction for low lying positive parity states of ^{87}Y. [NO] is the number of unpaired nucleons

E(th)	0.379	1.017	Orbit partition order				
[NO]	$9/2^+$	$5/2^+$	$\pi f_{5/2}$	$\pi p_{3/2}$	$\pi p_{1/2}$	$\pi g_{9/2}$	$\nu g_{9/2}$
[3]	1.09	1.30	5	3	2	1	8
[3]	14.61	12.91	5	4	1	1	8
[3]	7.14	18.61	6	3	1	1	8
[1]	77.16	67.18	6	4	0	1	8

Table 6. The spectroscopic factors S of low-lying states of ^{87}Y

	J^{π}	$1/2^-$	$3/2^-$	$5/2^-$	$9/2^+$
	E(MeV)	0.000	0.981	0.793	0.379
exp					
S[41]	(d,n)	0.570	0.1075	0.116	0.548
S[15]	$(^3He,d)$	0.575	0.135	0.192	0.719
th	j	$p_{1/2}$	$p_{3/2}$	$f_{5/2}$	$g_{9/2}$
S(j)	GWBXC	0.583	0.034	0.064	0.556
S(j)	PMM90	0.657	0.048	0.035	0.647

pair of neutrons in the $g_{9/2}$ shell. This situation does not seem to correspond to the experimental evidence coming from the spectroscopic factors of one-nucleon transfer reactions [15,41]. In fact, as shown in Table 6, while the calculation predicts large stripping spectroscopic S-factors for the $1/2^-$ and $9/2^+$ in good agreement with experiment, the calculated S-factors for the lowest $3/2^-$ and $5/2^-$ clearly underestimate the experimental values.

Given the restricted model space, any comparison with high-lying negative parity states is clearly ruled out. As regard to the positive parity states, interesting results have been obtained for the $5/2^+$ states, which show an appreciable agreement with the experimental data, for both the density of states and the energies of each individual state.

We turn now to the predictions of the PMM90 interaction. The main components of the lowest negative-parity states are given in Tables 7, 8, 9, 10, 11.

At variance with the case of the GWBXC interaction, the model space now allows for $2p-2h$ excitations of the core. One can see that, as in the case of GWBXC, the main component of the lowest $3/2^-$ state has a hole in the $2p_{1/2}$ orbital, while it is the third $3/2^-$ state to be associated mainly with the $2p_{3/2}$ orbital. As a consequence, the predicted stripping spectroscopic factor of the first $3/2^-$ state is still smaller than the experimental value (see Table 6). Note also that the highest states (the forth and fifth in the table) are completely associated with $2p-2h$ core excitations.

The situation is slightly different in the case of the $5/2^-$ states. In this case the amount of pure $f_{5/2}$ state in the lowest $5/2^-$ goes up to about 50%. Still the proton spectroscopic factor with respect to ^{86}Sr remains smaller than the experimental value (see Table 6).

As for the $1/2^-$ states (except the ground state), the $7/2^-$ and $9/2-$ states lying at high excitation energy (i.e. except the lowest state), the component associated with the $2p-2h$ excitation of the core is dominant.

As a general remark, as shown in Fig. 12, excluding the case of $1/2^-$ states, the calculated negative parity states compare well with the experimental levels. Due to the large model space with respect to the GWBXC case,

Table 7. Eigenvalues and percentage of different components within the shell model Hamiltonian with PMM90 interaction of the $1/2^-$ low-lying states of ^{87}Y. Each line corresponds to a state of the basis, which partition order is reported in the last four columns. [NO] is the number of unpaired nucleons. The percent occupations contributing more than 0.5% are reported in columns two, three and four

E(th)	0.000 [1]	2.105 [2]	2.497 [3]	Orbit partition order			
[NO]	p%	p%	p%	$f_{5/2}$	$p_{3/2}$	$p_{1/2}$	$g_{9/2}$
[3]	2.75	27.78	11.54	11	7	3	10
[1]	3.21	39.45	40.93	11	8	2	10
[1]	2.11	32.63	44.37	12	7	2	10
[1]	4.91			11	8	4	8
[1]	3.44			12	7	4	8
[1]	83.58		2.92	12	8	3	8

Table 8. The same as Table VII for the $3/2^-$ states of ^{87}Y

E(th)	0.900 [1]	1.278 [2]	1.993 [3]	2.228 [4]	2.611 [5]	Orbit partition order			
[NO]	p%	p%	p%	p%	p%	$f_{5/2}$	$p_{3/2}$	$p_{1/2}$	$g_{9/2}$
[3]	2.94	6.83	14.59	13.32	15.86	11	7	3	10
[1]	3.83	4.49	2.69	35.96	46.96	11	8	2	10
[1]	16.31	59.11	24.45	40.36	35.05	12	7	2	10
[1]	5.45	1.93	4.84			11	8	4	8
[1]	20.79	6.43	47.68	9.23		12	7	4	8
[1]	50.70	21.22	5.55			12	8	3	8

Table 9. The same as Table VII for the $5/2^-$ states of ^{87}Y

E(th)	0.738 [1]	1.167 [2]	1.604 [3]	2.007 [4]	2.582 [5]	Orbit partition order			
[NO]	p%	p%	p%	p%	p%	$f_{5/2}$	$p_{3/2}$	$p_{1/2}$	$g_{9/2}$
[3]	3.06	5.23	13.63	9.54	12.11	11	7	3	10
[1]	28.20	25.44	38.16	9.08	57.56	11	8	2	10
[1]	1.23	2.63		65.16	19.62	12	7	2	10
[1]	48.65	9.17	41.59	4.39	2.45	11	8	4	8
[1]	1.78	2.89		11.83	8.00	12	7	4	8
[1]	17.09	54.65	4.95			12	8	3	8

Table 10. The same as Table VII for the $7/2^-$ states of ^{87}Y

E(th)	1.397 [1]	1.735 [2]	2.082 [3]	2.312 [4]	2.465 [5]	2.741 [6]	Orbit partition order			
[NO]	p%	p%	p%	p%	p%	p%	$f_{5/2}$	$p_{3/2}$	$p_{1/2}$	$g_{9/2}$
[3]	3.41	8.67	13.82	12.57	8.99	20.00	11	7	3	10
[1]	6.37	48.00	7.17	38.57	8.16	33.56	11	8	2	10
[1]	4.14	5.45	64.28	10.84	61.27	40.31	12	7	2	10
[1]	11.85	31.61	9.04	33.39	8.00	4.88	11	8	4	8
[1]	6.29	1.54	1.44	4.57	10.60	1.25	12	7	4	8
[1]	67.94	4.74	4.25		2.97		12	8	3	8

Table 11. The same as Table VII for the $9/2^-$ states of ^{87}Y

E(th)	1.477 [1]	1.995 [2]	2.252 [3]	2.658 [4]	2.729 [5]	2.784 [6]	Orbit partition order			
[NO]	p%	p%	p%	p%	p%	p%	$f_{5/2}$	$p_{3/2}$	$p_{1/2}$	$g_{9/2}$
[3]	3.44	15.37	8.91	10.67	13.33	19.93	11	7	3	10
[1]	6.92	65.92	45.52	24.22	52.49	38.91	11	8	2	10
[1]	2.89	2.77	2.06	51.50	22.24	16.72	12	7	2	10
[1]	16.19	7.34	34.77	4.36	9.88	18.42	11	8	4	8
[1]	3.74		1.26	9.25	2.00	5.15	12	7	4	8
[1]	66.82	8.26	7.47				12	8	3	8

the number of predicted states is correct, and the discrepancy of the individual level energy is typically of the order of few hundred keV. A similar feature is not obtained for the positive parity states. Although in this case the model space is practically equivalent to the one of GWBXC interaction, the different matrix elements and the single particle energies lead to a set of states whose agreement with the experimental values is worse than in the case of GWBXC interaction.

As a final comment to this section, the results presented here confirm the difficulty of shell model calculations in giving a satisfactory account of the energy spectra in this region of nuclei, as one moves from the lowest excitation energy levels. The sensitivity of the results not only to the model space, but also to the interaction, clearly shows up from the comparison of both energy spectra and wave functions. The importance of $2p-2h$ excitations across the Z=40 subshell is confirmed by these calculations, in accordance with the situation in the neighbouring nuclei, as ^{90}Zr. In contrast to other features, we finally note that both interactions, in spite of the not complete closure of the shell, make similar predictions for the existence of different multiplets of states in ^{88}Y, which can be interpreted as homologous to corresponding parent states in ^{87}Y. Therefore these theoretical predictions strongly support the homologous state identification performed by shape comparison of the cross section and asymmetry experimental angular distributions in ^{90,91}Zr$(\vec{p},\alpha)$ reactions [6].

6 Conclusions

Cross sections and asymmetry angular distributions have been measured in a high resolution experiment for transitions to 36 levels of ^{87}Y up to an excitation energy of about 3 MeV in the $(\vec{p},\alpha)$ reaction induced on ^{90}Zr at 22 MeV proton incident energy.

Using Woods-Saxon and Double-Folded potentials for the α exit channel, two different analyses, with comparable accuracy, of the experimental reaction data have been performed. Exploiting the noticeable dependence on the transferred total angular momentum J, displayed by $\sigma(\theta)$ and, in a larger degree, by $A_y(\theta)$ we have made 25 unambiguous attributions of J^π, which represent a considerable improvement of the knowledge of the ^{87}Y level scheme.

In order to achieve a better understanding of the region of nuclei with A$\sim$ 90, the present $(\vec{p},\alpha)$ data have been supplemented with shell model calculations for the residual ^{87}Y nucleus, utilizing the large-basis shell model code OXBASH.

For the ^{87}Y nucleus the structure of both low-lying and highly excited states and one-nucleon stripping spectroscopic factors respect to ^{86}Sr, has been studied using two different interactions, the GWBXC and PMM90. The results achieved confirm the importance of $2p-2h$ excitations across the Z=40 subshell.

Furthermore, both interactions make similar theoretical predictions for the occurrence in ^{88}Y of different multiplets of states, whose wave functions are similar to the wave functions of corresponding low-lying parent states in ^{87}Y, in agreement with the experimental findings in ^{90,91}Zr$(\vec{p},\alpha)$ reactions [6].

Two of the authors (J.N.G. and M.J.) would like to acknowledge the Istituto Nazionale di Fisica Nucleare for its support. This work was supported in part by grants of the Italian MURST and of the DFG under C4-Gr894/2.

References

1. E. Gadioli and P.E. Hodgson, Rep. Prog. Phys. **52**, (1989) 247
2. R.J. Peterson and H. Rudolph, Nucl. Phys. **A241**, (1975) 253;
   R. Muller, Thesis, Univ.München (1973)
3. E. Gadioli, P. Guazzoni, S. Mattioli, L. Zetta, G. Graw, R. Hertenberger, D. Hofer, H. Kader, P. Schiemenz, R. Neu, H. Abele and G. Staudt, Phys. Rev. **C43**, (1991) 2572
4. E. Gadioli, P. Guazzoni, M. Jaskola, L. Zetta, G. Colombo, G. Graw, R. Hertenberger, D. Hofer, H. Kader, P. Schiemenz, R. Neu and G. Staudt, Phys. Rev. **C47**, (1993) 1129
5. P. Guazzoni, M. Jaskola, L. Zetta, G. Graw, R.Hertenberger, D.Hofer, P. Schiemenz, U.Atzrott, R.Neu and G.Staudt, Phys. Rev. **C49**, (1994) 2784
6. P. Guazzoni, M. Jaskola, L. Zetta, J. Gu, A. Vitturi, G. Graw, R. Hertenberger, D. Hofer, P. Schiemenz, B. Valnion, U. Atzrott, G. Staudt, Gh. Cata-Danil, Zeit. Phys. **A356**, (1997) 381
7. P. Guazzoni, U. Atzrott, Gh. Cata-Danil, G. Graw, R. Hertenberger, D. Hofer, M. Jaskola, P. Schiemenz, G. Staudt, J. Tropilo, E. Zanotti-Müller and L. Zetta, *Polarization Phenomena in Nuclear Physics*, 8^{th} International Symposium, Bloomington, IN 1994, AIP CONFERENCE PROCEEDINGS 339, p.569 and Report INFN/BE-96/09 (1996)
8. P.Guazzoni, L.Zetta, P.Demetriou and P.E.Hodgson, Zeit. Phys. **A354**, (1996) 53
9. J.L. Irigaray, M. Asghar, J. Dalmas, G.Y. Petit and J. Roturier, Nucl. Phys. **A136**, (1969) 631
10. C.A. Fields, F.W.N. de Boer, J.J. Kraushaar, W.W. Pratt, R.A. Ristinen and I.E. Samuelson, Z. Phys. **A295**, (1980) 365
11. E.K. Warburton, J.W. Olness, C.J. Lister, J.A. Becker and S.D. Bloom, J. Phys. G **12**, (1986) 1017
12. L.K. Kostov, W. Andrejtscheff, L.G. Kostova, P. Petkov, L. Funke, L. Käubler and H. Prade, Z. Phys. **A330**, (1988) 45
13. F. Meurders, W.P.T.M. van Eeghem and P. Spilling, Nucl. Phys. **A196**, (1972) 353
14. H.T. King and D.C. Slater, Nucl. Phys. **A283**, (1977) 365
15. J.V. Mahrer, J.R. Comfort and G.C. Morrison, Phys. Rev. **C3**, (1971) 1162
16. R.J. Peterson and H. Rudolph, Nucl. Phys. **A202**, (1973) 335
17. J.R. Comfort, A.M. Nathan, W.J. Braithwaite and J.R. Duray, Phys. Rev. **C11**, (1975) 2012

18. I.C. Oelrich, K. Krien, R.M. DelVecchio and R.A. Naumann, Phys. Rev. **C14**, (1976) 563
19. L.R. Medsker, D. Mukhopadhyay and H.T. Fortune, Nucl. Phys. **A292**, (1977) 61
20. H. Sievers, Nuclear Data Sheets **62**, (1991) 327
21. E. Zanotti, M. Bisenberger, R. Hertenberger, H. Kader and G. Graw Nucl. Instr. and Meth. **A310**, (1991) 706
22. J.R. Comfort, ANL Physics Division, Report N.PHY19708, Argonne
23. M. Igarashi, TWOFNR code, unpublished
24. R.L. Varner, W.J. Thompson, T.L. McAbee, E.L. Ludwig and T.B. Clegg, Phys. Rep.**201**, (1991) 57
25. M. Wit, J. Schiele, K.A. Eberhard and J.P. Schiffer, Phys. Rev. **C12**, (1975) 1447
26. A.M. Kobos, B.A. Brown, R. Lindsay, and G.R. Satchler, Nucl. Phys. **A425**, (1984) 205
27. H. de Vries, C.W. de Jager, and C. de Vries, At. Data Nucl. Data Tables **36**,(1987) 495
28. G.R. Satchler, and W.G. Love, Phys. Rep. **55**,(1979) 183
29. H. Abele, H.J. Hauser, A. Korber, W. Leitner, R. Neu, H. Plappert, T. Rohwer, G. Staudt, M. Strasser, S. Welte, M. Walz, P.D. Eversheim, and F. Hirterberger, Z.Phys.**A326**, (1987) 373
30. P.D. Kunz, computer code DWUCK5, University of Colorado, unpublished
31. M. Walz, computer code TROMF, University of Tübingen, unpublished
32. M. Walz, R. Neu, G. Staudt, H. Oberhummer, and H. Cech, J. Phys. **G 14**, (1988) L91
33. J.B. Ball, C.B. Fulmer, and R.H. Bassel, Phys. Rev. **135**, (1964) B706
34. U. Atzrott, P. Mohr, H. Abele, C. Hillenmayer, and G. Staudt, Phys. Rev. **C53**, (1996) 1336
35. J.B.A. England, S. Baird, D.H. Newton, T. Picazo, E.C. Pollacco, G.J. Pyle, P.M. Rolph, J. Alabau, E. Casal, and A. Garcia, Nucl. Phys. **A388** (1982), 575
36. Y. Tagishi, K. Katori, M. Sasagase, M. Sato, T. Aoki and T. Mikumo, Phys. Rev. Letters **41**, (1978) 16
37. R.N. Boyd, E. Sugarbaker, S.L. Blatt, T.R. Donoghue and H.J. Hausman, Nucl. Phys.**A372**, (1981) 51
38. J.Sinatkas, L.D.Skouras, D.Strottman and J.D.Vergados, J.Phys.G: Nucl. Part. Phys.**18**, (1992) 1377;
J.Sinatkas, L.D.Skouras, D.Strottman and J.D.Vergados, J.Phys.G: Nucl. Part. Phys.**18**, (1992) 1401
39. B.A. Brown, A. Etchegoyen and W.D.M. Rae, MSU-NSCL Report No. 524 (1985)
40. A. Hosaka, K.-I. Kubo and H. Toki, Nucl. Phys.**A444**, (1985) 76
41. J.L. Horton and C.E. Hollandsworth, Phys. Rev. **C13**, (1976) 2212